A GENERAL EMPIRICALLY BASED MICROINSTABILITY TRANSPORT MODEL

G. VLAD, M. MARINUCCI, F. ROMANELLI
Associazione Euratom–ENEA sulla Fusione,
C.R. Frascati, Frascati, Rome,
Italy

A. CHERUBINI, M. ERBA, V.V. PARAIL, A. TARONI
JET Joint Undertaking,
Abingdon, Oxfordshire,
United Kingdom

ABSTRACT. A mixed Bohm–gyro-Bohm, shear dependent thermal diffusion coefficient to model the anomalous thermal transport in tokamaks is proposed. It is derived on the basis of recent findings on the radial correlation length of turbulent processes generated by small scale, collisionless, electrostatic microinstabilities (Romanelli, F., Zonca, F., Phys. Fluids B **5** (1993) 4081). The model has been used to describe standard L and H mode discharges of the JET, DIII-D and TFTR devices and JET pellet enhanced performance (PEP) and hot ion mode discharges successfully.

1. INTRODUCTION

The energy and particle transport in tokamaks is determined by turbulent processes. At present, no definitive transport model (i.e. a closed expression for energy and particle fluxes in terms of plasma parameters) that fully accounts for all the features of turbulence is available, in spite of the effort spent in recent years to determine the anomalous fluxes from first principle plasma models [1–5]. Nevertheless, there is a broad consensus about the fact that the underlying mechanism is associated with the presence of small scale instabilities, in particular those belonging to the drift branch and destabilized by the free energy sources related to the density and temperature gradients.

Semiempirical transport models have been developed, based on the most important features of the linear dynamics of the electrostatic instabilities. Most of the transport models proposed so far have considered simple gyro-Bohm expressions for the transport coefficients [1, 4, 6],

$$\chi_{\mathrm{GB}} \approx \rho_{\mathrm{i}}^2 \omega_* . \tag{1}$$

The underlying idea is that turbulent transport is characterized by a radial correlation length L_r of the order of the ion gyroradius ρ_{i} and by a decorrelation rate of the order of the diamagnetic frequency $\omega_* \approx v_{\mathrm{ti}}/a$ (v_{ti} being the ion thermal velocity and a the minor radius), as expected for the microinstabilities of the drift branch. On the contrary, the presence of turbulent processes with long radial correlation lengths (say, $L_r \approx (a\rho_{\mathrm{i}})^{0.5}$) would result in Bohm, rather than gyro-Bohm, transport,

$$\chi_{\mathrm{B}} \approx \rho_{\mathrm{i}} v_{\mathrm{ti}} . \tag{2}$$

However, it has been shown in several experiments that both the local transport and the energy confinement time can exhibit a behaviour that, depending on the confinement regime, may be clearly different from gyro-Bohm behaviour. To be specific, it has been shown on DIII-D [7] that the ion transport can change from gyro-Bohm in H mode discharges with narrow current profiles to the so-called 'Goldston' regime, $\chi \propto \rho_{\mathrm{i}}^{1/2}$ (i.e. with a weaker than Bohm ρ_{i} dependence) in L mode discharges with broad current density profiles. On JET, a one fluid analysis shows that the energy transport is Bohm in L mode discharges [8] and gyro-Bohm in H mode discharges [9]. In addition, on TFTR, a one fluid analysis shows that the energy transport is Bohm in L mode discharges [10].

As shown in Ref. [11], such a change can be explained in terms of a pure gyro-Bohm model; however, more subtle mechanisms such as the neutral dynamics at the plasma edge, which affects the density profile shape, must be considered. On the basis of this observation, in Ref. [12] a mixed Bohm–gyro-Bohm model has been proposed, generalizing the previous Bohm model [13].

The fact that transport can show different scalings raises the question of whether simple theory based transport models may be, in fact, used to describe tokamak transport. Within the context of simple mixing length arguments, this is equivalent to asking whether the same turbulent process can exhibit conditions in which the radial correlation length of turbulence has different scalings with the gyroradius.

As shown in Refs [14, 15], electrostatic instabilities in tokamaks are indeed characterized by two scale lengths during the linear phase of the instabilities. A general perturbation in a two dimensional (2-D) equilibrium, such as a tokamak equilibrium, can be decomposed in Fourier harmonics $\propto \exp(\mathrm{i}\, m\theta - \mathrm{i}\, n\phi)$ along the poloidal (θ) and toroidal (ϕ) angles (here m, n are, respectively, the poloidal and toroidal mode numbers) and is given by a superposition of different poloidal harmonics corresponding to the same toroidal mode number n. Different poloidal harmonics are linearly coupled owing to the poloidal variation of the equilibrium, mostly due to the effect of toroidicity. In the high-n limit, each poloidal harmonic m is almost identical to its neighbouring harmonics $m \pm 1$, being simply radially shifted by an amount $\Delta r \equiv 1/nq'$, corresponding to the distance to neighbouring mode rational surfaces, since each harmonic tends to localize around its mode rational surface in order to minimize the effect of parallel compressibility (here q is the safety factor and the prime represents the derivative with respect to the radial co-ordinate). The typical width of a single poloidal harmonic is of the order of the ion gyroradius. On a longer radial scale, the superposition of different poloidal harmonics is modulated by an envelope with a characteristic width that depends on the global shape of the equilibrium profiles and turns out to be of the order of $(a\rho_\mathrm{i})^{1/2}$. However, the latter width depends on the degree of coupling between neighbouring harmonics. If the coupling tends to weaken, each harmonic tends to behave in an independent way with respect to the others.

On the basis of the above findings, it is natural to propose the following picture. Let us suppose that the instability maintains a memory of the linear coupling also in the turbulent phase. In such a case, if the coupling is strong, the radial correlation length may be identified with the envelope width, yielding Bohm transport. Conversely, if the coupling is weak, the radial correlation length may be identified with the width of a single poloidal harmonic, yielding gyro-Bohm transport.

Therefore, tokamak transport may in principle be modelled by a superposition of a Bohm contribution and a gyro-Bohm contribution, one being dominant depending on the degree of coupling between poloidal harmonics.

The degree of coupling may be associated with different physical mechanisms. The model that is presented here relies on the simplest mechanism, which is related to the effect of magnetic shear. Indeed, as shown in Ref. [14], if the magnetic shear parameter $s \equiv rq'/q$ is decreased, the distance between neighbouring harmonics, Δr, increases faster than the width of the eigenfunction, leading to a decrease in the overlap between neighbouring harmonics and, ultimately, the degree of coupling. Thus, if a large region of weak shear is obtained, a corresponding decrease of transport from Bohm to gyro-Bohm is expected. Preliminary confirmation of this idea in the analysis of the behaviour of the impurity transport has been obtained in Ref. [16].

It should be noted that the effect of magnetic shear is not the only factor in principle able to affect the overlap between neighbouring harmonics. For example, the effect of a sheared poloidal flow may play a similar role, as expected in the case of the L–H transition. However, owing to the lack of a simple model for sheared flow generation, in the present article H mode discharges will be simulated by imposing boundary conditions for the temperatures inside the 'pedestal' region, with no attempt to describe it.

The beneficial effect of reduced magnetic shear has been observed in several experimental conditions. A strong reduction of transport is currently observed in the central part of tokamak discharges, where magnetic shear is low, if sawteeth are suppressed. Perhaps the first experimental evidence was found with the pellet enhanced performance (PEP) mode in JET [17], in which the injection of a deuterium pellet yielded a flattening of the safety factor profile inside the deposition region. Confinement enhancements with pellet injection have been reported in several tokamaks [18–20], even though usually attributed to the peaking of the density profile, rather than to changes of the safety factor profile. More recently, confinement improvement has been observed in the presence of large regions of low or reversed shear produced by lower hybrid current drive [21], or by freezing the current density profile by strong auxiliary heating during current ramp [22–24]. In the present article, we will check the model against some selected discharges from the ITER Profile

Database and against the JET PEP and hot ion mode discharges.

The structure of this article is as follows: in Section 2, a mixed Bohm–gyro-Bohm, magnetic shear dependent model will be presented; in Section 3, a transport code will be used to simulate experimental discharges ('standard' L and H mode discharges from the ITER Profile Database in Section 3.1, and JET PEP and hot ion mode discharges in Section 3.2). Finally, some conclusions will be drawn in Section 4.

2. A MAGNETIC SHEAR DEPENDENT TRANSPORT MODEL

We discuss here the construction of a mixed Bohm–gyro-Bohm, shear dependent transport model following the findings mentioned in the previous section. As already stated in Section 1, a crude estimate is often made for the thermal diffusion coefficient χ, employing the so-called mixing length argument, $\chi \approx L_r^2/\tau_c$, where L_r is the mode radial correlation length and τ_c the autocorrelation time of the turbulent fields associated with the considered instability. Referring to small scale, collisionless, electrostatic microinstabilities (e.g., ion temperature gradient driven (ITG) modes), τ_c can be identified as the inverse of the diamagnetic frequency ω_T^* associated with the temperature gradient,

$$\tau_c^{-1} \approx \omega_T^* = \frac{k_\theta T}{B L_T} \tag{3}$$

where k_θ is the wave vector along the poloidal direction, B is the magnetic field and $L_T^{-1} \equiv |\nabla T|/T$ is the inverse of the characteristic length of the temperature profile.

Assuming $k_\theta \propto \rho_i^{-1}$ and estimating L_r as the perpendicular wavelength of the mode, which for the class of microinstabilities considered above is of the order of the ion Larmor radius (calculated at the electron temperature T_e), ρ_s (m) $\equiv \sqrt{m_i T_e}/(eB) = 1.02\times10^{-4}\sqrt{T_e\ (\mathrm{eV})}/B$ (T), one obtains for the thermal diffusion coefficient the following expression:

$$\chi \propto D_B \rho^* \frac{1}{L_T^*} \tag{4}$$

where D_B (m^2/s) $\equiv T_e(\mathrm{eV})/16B(\mathrm{T})$ is the Bohm diffusion coefficient, $\rho^* \equiv \rho_s/a$ and $L_T^* \equiv L_T/a$ are, respectively, the gyroradius and the characteristic length of the temperature profile, both normalized to the minor radius of the plasma column a. Because of the linear dependence of χ on ρ^* in Eq. (4), this type of thermal diffusion coefficient is usually referred to as 'gyro-Bohm' [25].

As already discussed in Ref. [14], thermal diffusion coefficients of the gyro-Bohm type typically decrease towards the edge of the discharge, whereas the opposite dependence is observed experimentally. In Ref. [14] it has been pointed out that the above mentioned disagreement can be traced back to the estimate of the radial correlation length L_r. Indeed, as already mentioned in Section 1, the presence of turbulent processes with long radial correlation lengths would result in Bohm-like transport,

$$\chi \propto D_B \frac{1}{L_T^*}\,. \tag{5}$$

Radially elongated structures are observed experimentally [26] and numerically [5, 27] in the turbulent fields of tokamak discharges.

Indeed, in Ref. [14], the radial correlation length in the short wavelength, moderate shear limit has been found to scale as $L_r \propto s^{-1/2}$. This is true as long as the toroidal coupling between different poloidal harmonics is sufficiently strong to produce a radial correlation length that is larger than the width of each poloidal harmonic of the mode. If such a condition is not satisfied, as in the long wavelength, low shear limit, the radial correlation length has been found to scale as $L_r \propto \mathrm{e}^{-1/s}$, thus vanishing very rapidly for decreasing shear; then the radial correlation length must be identified with the width of the single (decoupled) poloidal harmonic. This, in turn, scales as the ion Larmor radius, thus giving rise to a gyro-Bohm scaling of the thermal diffusion coefficient.

Following these theoretical suggestions, a thermal diffusion coefficient can be modelled assuming a Bohm-like dependence in the radial regions where the magnetic shear is $s \geq 1$ and which vanishes with decreasing s, and a gyro-Bohm-like dependence which survives where the shear $s \ll 1$.

Following Refs [25, 28], we write the thermal diffusion coefficient as

$$\chi = D_B F(\rho^*, L_T^*, q, s) \tag{6a}$$

in which

$$F(\rho^*, L_T^*, q, s) = \alpha_B \frac{1}{L_T^*} q^2 f(s) + \alpha_{gB} \rho^* \frac{1}{L_T^*} \tag{6b}$$

where $f(s)$ is a function that depends only on the magnetic shear and α_B and α_{gB} are numerical coefficients used for calibration, which multiply the Bohm

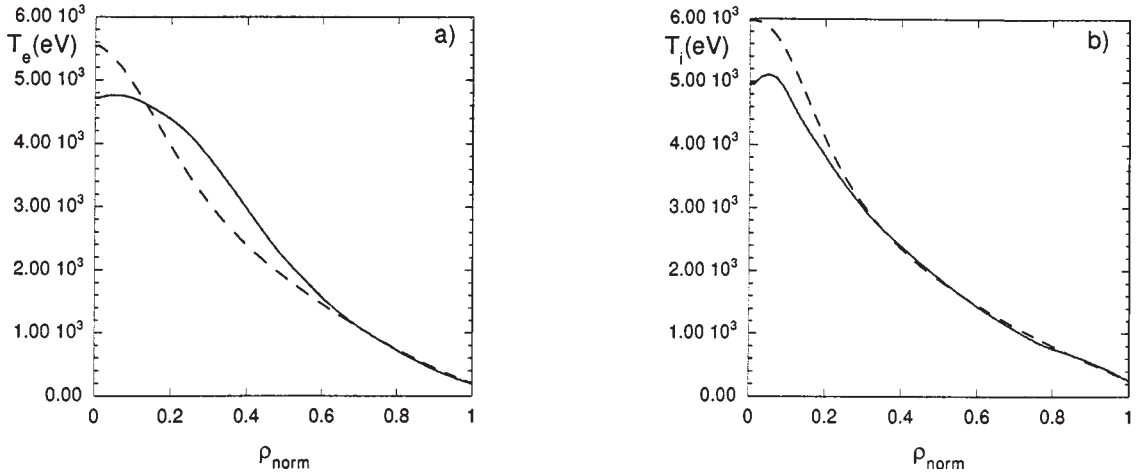

FIG. 1. Experimental (solid curves) and computed (dashed curves) electron (a) and ion (b) temperature profiles for JET discharge 19649 at $t \simeq 50$ s.

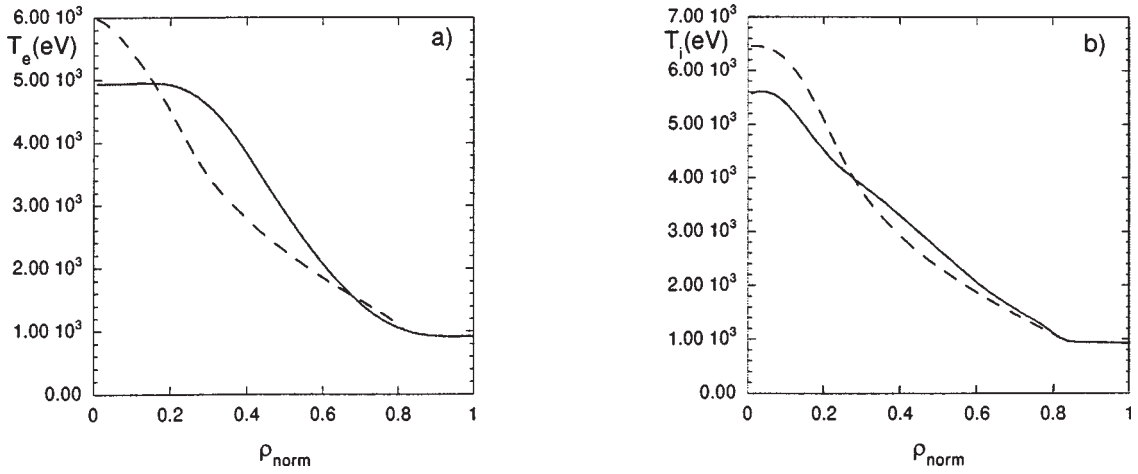

FIG. 2. Experimental (solid curves) and computed (dashed curves) electron (a) and ion (b) temperature profiles for JET discharge 19691 at $t \simeq 54$ s.

and gyro-Bohm parts, respectively, of the thermal diffusion coefficient. The quadratic dependence on the safety factor q that appears in the Bohm part of the thermal coefficient was found to be necessary [13] to better represent the experimental data from JET. This choice, as discussed in Ref. [13], results in a linear q dependence of the energy confinement time and agrees with the current ramp experiment in JET [24]. It also properly models the observed increase towards the plasma edge of the thermal diffusion coefficient. For the shear dependent function $f(s)$, the following expression has been chosen:

$$f(s) = s^2/(1+|s|^3) \qquad \text{if} \qquad s > 0 \tag{7a}$$

$$f(s) = 0 \qquad \text{if} \qquad s \leq 0. \tag{7b}$$

This choice respects the desired dependence of the radial correlation length $L_r \propto s^{-1/2}$ in the moderate shear limit and makes the radial correlation length vanish as s goes to zero. If the shear profile is flat or even 'reversed' (as can happen in the central part of the discharge), the Bohm term of the model thermal diffusion coefficient is cut off and the transport is of the purely gyro-Bohm type.

The thermal coefficients for electrons and ions are then assumed to be

$$\chi_{\mathrm{e}} = \alpha_{\mathrm{B,e}} D_{\mathrm{B}} \frac{1}{L^*_{T_{\mathrm{e}}}} q^2 f(s) + \alpha_{\mathrm{gB}} D_{\mathrm{B}} \rho^* \frac{1}{L^*_{T_{\mathrm{e}}}} \tag{8a}$$

$$\chi_{\mathrm{i}} = \alpha_{\mathrm{B,i}} D_{\mathrm{B}} \frac{1}{L^*_{T_{\mathrm{i}}}} q^2 f(s) + \alpha_{\mathrm{gB}} D_{\mathrm{B}} \rho^* \frac{1}{L^*_{T_{\mathrm{i}}}} + \chi_{\mathrm{neo}} \quad (8\mathrm{b})$$

where χ_{neo} is the neoclassical ion thermal diffusion coefficient [29] and the three calibration constants have been tuned for a typical L mode JET discharge,

$$\alpha_{\mathrm{B,e}} = 8.61 \times 10^{-3}, \qquad \alpha_{\mathrm{B,i}} = 3.5\alpha_{\mathrm{B,e}} \quad (9\mathrm{a})$$

$$\alpha_{\mathrm{gB}} = 5.07 \times 10^{-1}. \quad (9\mathrm{b})$$

In the following, these calibration constants will be kept fixed for all the simulations performed.

3. TRANSPORT SIMULATIONS AND COMPARISON WITH EXPERIMENTS

The semiempirical transport model described in Section 2 has been inserted in the transport code JETTO [30] in order to compare its predictions with experimental results. To better focus on the results of the thermal transport coefficient proposed, the code has been operated in a semi-interpretative mode. That is, we have solved the ion and electron energy conservation equations together with the evolution of the Faraday equation, assuming neoclassical resistivity and including the bootstrap current. Ohmic input, thermal exchange between electrons and ions, and power losses via thermal diffusion are calculated self-consistently (convection losses have been neglected). The other quantities that enter the transport equations (e.g., profiles of density, Z_{eff}, auxiliary power deposition and radiation power) have been prescribed according to the experimental database. In addition, the equilibrium quantities necessary to solve the transport equations have been assigned according to the experimentally reconstructed equilibria. Moreover, no sawtooth model has been included in the simulations, there often not being detailed experimental information available. The boundary conditions for the electron and ion temperatures have been imposed as being equal to the experimental values. They have been imposed at a radial position that varies in the range $\rho_{\mathrm{norm}} = 0.8$–$1.0$ (here ρ_{norm} is the square root of the normalized toroidal flux, the radial variable used by JETTO), depending on the discharge (often, the experimental profiles provided for the temperature measurements lose accuracy in the outermost part of the plasma column). The total current, as obtained from the database, has been imposed as a boundary condition for the Faraday equation, and, when available, the current density driven by the neutral beam has been prescribed (it has to be noted that for all the discharges considered hereafter, the neutral beam driven current density is a small fraction of the total current density). Moreover, the initial conditions for the T_{e}, T_{i} and q profiles have been taken from the experimental database.

3.1. ITER Profile Database discharges

In this section, we present a comparison of the magnetic shear dependent transport model described in Section 2 with some of the experimental results collected in the ITER Profile Database [31]. In particular, results of simulations of L mode JET, DIII-D and TFTR discharges and H mode JET and DIII-D discharges will be presented. It should be noted that all the discharges considered have a much larger auxiliary heating than ohmic heating.

In Fig. 1, the computed electron and ion temperatures are shown compared with the experimental temperature profiles for JET discharge 19649 at $t \simeq 50$ s. This is a typical steady state JET L mode discharge.

In Fig. 2, the computed electron and ion temperatures are shown compared with the experimental temperature profiles for JET discharge 19691 at $t \simeq 54$ s. This is a typical steady state JET L mode discharge similar to discharge 19649 but with the auxiliary power almost doubled. The simulation has been started from the ohmic phase, just before the neutral beam auxiliary power is switched on, and followed until the quasi-steady-state L phase is reached (Fig. 2).

For both the JET discharges analysed here a good agreement with the ion experimental profiles is obtained, whereas the computed electron temperature profiles are more peaked than the experimental ones. Indeed, if a sawtooth mechanism were included in the simulations, flatter temperature profiles would be obtained in the central region of the discharges.

Several L and H mode discharges from the ITER Profile Database have been analysed, the parameters of which are summarized in Table I.

The two discharges at high ρ^* (69627 and 71378b) and central neutral beam depositions are very well reproduced. We present in the following the results regarding DIII-D discharge 69627. In Fig. 3, the steady state computed temperature profiles are compared with the experimental ones for this discharge. In Fig. 4, the self-consistently computed safety factor and magnetic shear profiles are shown, together with the shear dependent function $f(s)$ (Eqs 7(a, b)). The safety factor profile as obtained from the ITER Profile Database is also shown for comparison: the

Table I. ITER Profile Database L and H Mode Discharges Analysed

Device/discharge	t (s)	$\langle n_e \rangle \times 10^{20}$ (m^{-3})	$T_e(0)$ (keV)	B_T (T)	I_p (MA)	P_{NB} (MW)	Phase, notes
JET/19649	50.0	0.35	5.5	3.1	3.0	9.0	L[a]
JET/19691	54.0	0.48	6.0	3.0	3.0	18.0	L
DIII-D/69627	2.4	0.39	1.93	1.01	1.01	3.3 (on-axis)	L, high ρ^*
DIII-D/69648	4.1	0.96	2.74	1.98	2.01	15.3 (flat)	L, low ρ^*
DIII-D/71378a	2.98	0.37	1.80	1.00	0.70	3.5 (off-axis)	L, high ρ^*
DIII-D/71378b	3.45	0.35	2.04	1.00	0.69	3.5 (on-axis)	L, high ρ^*
DIII-D/71384	3.45	0.89	3.25	2.00	1.39	3.3 (flat)	L, low ρ^*
TFTR/45950	4.53	0.33	5.43	4.8	2.0	11.4	L
TFTR/50862	3.52	0.24	5.44	3.6	1.5	11.8	L, low ν^*
TFTR/50903	3.92	0.22	4.38	2.9	1.2	9.4	L, medium ν^*
TFTR/50904	3.84	0.26	4.17	2.9	1.2	7.2	L, medium ρ^*
TFTR/50911	3.92	0.44	4.46	4.3	1.8	17.7	L, low ρ^*
TFTR/50921	3.84	0.18	3.08	2.2	0.89	4.5	L, high ρ^*
TFTR/52527	3.88	0.23	2.67	2.2	0.89	4.28	L, high ν^*
JET/33131	55.7	0.71	6.36	3.1	2.8	18.0	HGELM[b], low ρ^*
JET/33140	56.5	0.37	3.7	1.8	1.6	5.7	HSELM[c], high ρ^*
DIII-D/77557	2.7	0.49	3.04	2.0	0.99	4.73	HSELM
DIII-D/77559	2.7	0.49	3.04	2.0	0.99	4.73	HSELM
DIII-D/82205	3.66	0.53	4.34	1.9	1.34	5.86	HSELM, low ρ^*
DIII-D/82788	3.54	0.29	2.35	0.94	0.66	3.25	HSELM, high ρ^*

[a] L mode.
[b] H mode with large ELMs.
[c] H mode with small ELMs.

experimental and computed profiles are very similar, the main observable difference being a vertical shift that can be related to small differences in the equilibrium reconstruction (the physical boundary condition imposed in the simulations is on the total plasma current and not the safety factor at the edge). In Fig. 5, the total electron and ion thermal diffusion coefficients are shown, together with the Bohm, gyro-Bohm and neoclassical (for ions) contributions. Figure 5 clarifies the role of the shear dependent function $f(s)$, which tends to switch off the Bohm term in the central region of the discharge where the magnetic shear is low. In the same region the effect of the gyro-Bohm term can become dominant. In the central region of the discharge the ion thermal diffusivity is dominated by the neoclassical term.

On the contrary, the model is not able to reproduce the temperature profiles classified as discharge 71378a. This time slice of discharge 71378 differs from the time slice classified as 71378b because of the neutral beam deposition profile, which in this case is off-axis. Our model gives, as a result, temperature profiles that are very flat in the central region, whereas the experimental ones are peaked. The two discharges at low ρ^* (69648 and 71384) are well reproduced in the shape of the temperature profiles, but somewhat underestimated in their peak values. In Fig. 6, the standard deviation

$$\sigma_{T_{i,e}} = \frac{\left(\sum_{\rho_{norm}^{min}}^{\rho_{norm}^{max}} (T_{i,e,sim} - T_{i,e,exp})^2\right)^{1/2}}{\left(\sum_{\rho_{norm}^{min}}^{\rho_{norm}^{max}} T_{i,e,exp}^2\right)^{1/2}} \quad (10)$$

for the ion and electron temperature profiles are shown (respectively, σ_{T_i} and σ_{T_e}). Two values are given for each species, the one corresponding to the whole discharge ($\rho_{norm}^{min} = 0$ and $\rho_{norm}^{max} = 1$) and the one corresponding to the so-called 'good confinement region', here considered to be represented by the plasma volume ranging between $\rho_{norm}^{min} = 0.3$ and $\rho_{norm}^{max} = 0.8$. The mean values of the temperature standard deviations for all the discharges simulated are the following:

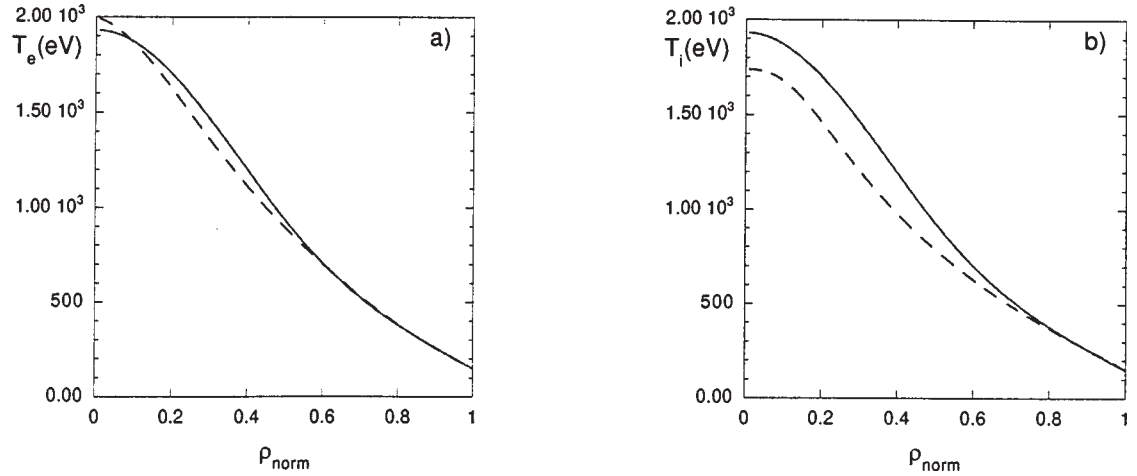

FIG. 3. Experimental (solid curves) and computed (dashed curves) electron (a) and ion (b) temperature profiles for DIII-D discharge 69627 at $t \simeq 4.4$ s.

$$\langle \sigma_{T_e} \rangle \Big|_0^1 = 0.215, \qquad \langle \sigma_{T_i} \rangle \Big|_0^1 = 0.214$$

$$\langle \sigma_{T_e} \rangle \Big|_{0.3}^{0.8} = 0.182, \qquad \langle \sigma_{T_i} \rangle \Big|_{0.3}^{0.8} = 0.173.$$

In Fig. 7, the ratios between the simulated (W_s) and the experimental (W_x) electron, ion and total (electrons plus ions) stored thermal energies are shown for all the discharges considered above. The same quantities that refer to the so-called 'good confinement region' are also presented. The mean values of W_s/W_x for all the discharges simulated and the quantities

$$\Delta R_W = \left(\sum_{i=1}^{N} (W_{s,i}/W_{x,i} - 1)^2 / N \right)^{1/2}$$

(where N is the number of discharges) are the following:

$$\left\langle \frac{W_{s,e}}{W_{x,e}} \right\rangle \Big|_0^1 = 1.01, \qquad \left\langle \frac{W_{s,i}}{W_{x,i}} \right\rangle \Big|_0^1 = 0.89$$

$$\left\langle \frac{W_s}{W_x} \right\rangle \Big|_0^1 = 0.95, \qquad \Delta R_{W,e} \Big|_0^1 = 19.26\%$$

$$\Delta R_{W,i} \Big|_0^1 = 17.56\%, \qquad \Delta R_W \Big|_0^1 = 16.20\%$$

$$\left\langle \frac{W_{s,e}}{W_{x,e}} \right\rangle \Big|_{0.3}^{0.8} = 1.00, \qquad \left\langle \frac{W_{s,i}}{W_{x,i}} \right\rangle \Big|_{0.3}^{0.8} = 0.91$$

$$\left\langle \frac{W_s}{W_x} \right\rangle \Big|_{0.3}^{0.8} = 0.96, \qquad \Delta R_{W,e} \Big|_{0.3}^{0.8} = 17.96\%$$

$$\Delta R_{W,i} \Big|_{0.3}^{0.8} = 16.09\%, \qquad \Delta R_W \Big|_{0.3}^{0.8} = 15.74\%.$$

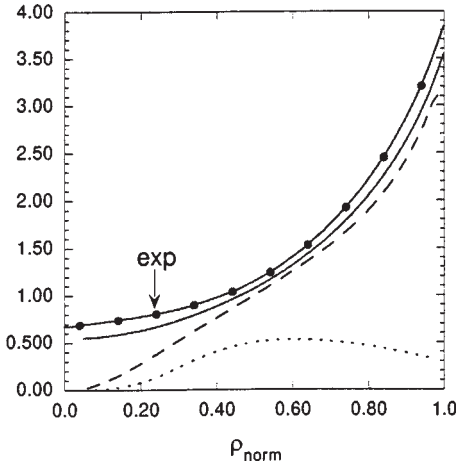

FIG. 4. Safety factor q (solid curve), shear (dashed curve) and shear dependent function $f(s)$ (dotted curve) radial profiles for the same discharge as Fig. 3. The safety factor as obtained from the ITER Profile Database is also shown for comparison (solid curve with filled circles labelled 'exp').

As a general comment, the simulated stored energies for the L mode TFTR discharges tend to be higher than the experimental ones, as can be seen from Fig. 7, whereas the JET and DIII-D discharges exhibit the opposite trend. This could suggest an explicit dependence of transport on elongation that

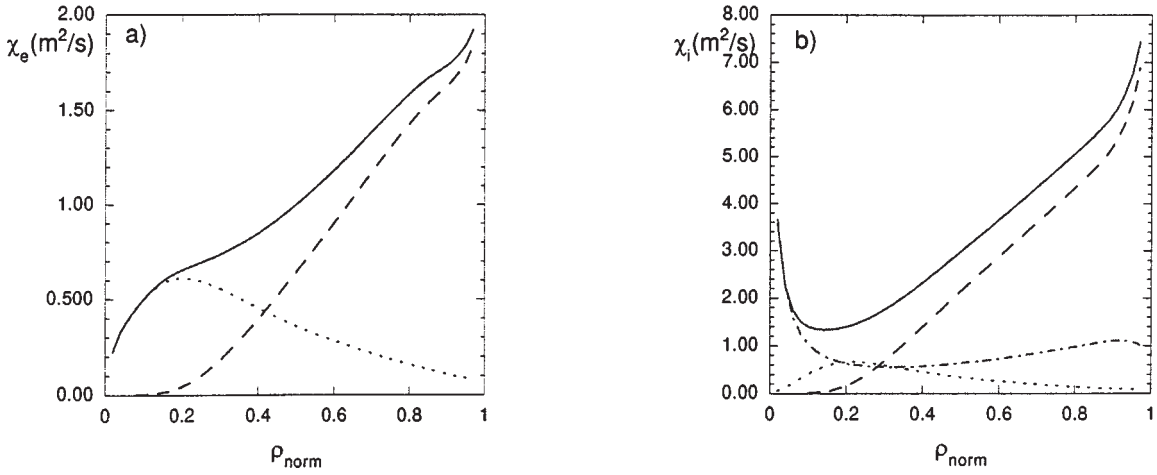

FIG. 5. Total (solid curves) electron (a) and ion (b) thermal diffusivity radial profiles and Bohm (dashed curves), gyro-Bohm (dotted curves) and ion neoclassical (chain curve) contributions for the same discharge as Fig. 3.

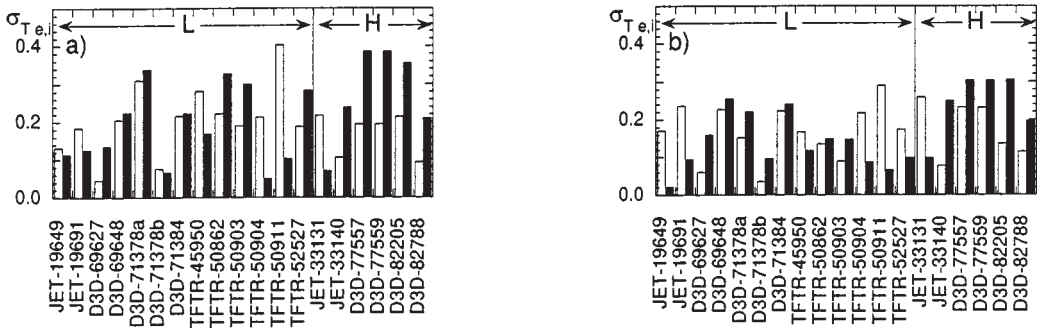

FIG. 6. Electron (white columns) and ion (black columns) temperature standard deviations for the discharges simulated: (a) on the whole cross-section ($\rho_{\rm norm} \in [\rho^{\rm min}_{\rm norm}, \rho^{\rm max}_{\rm norm}] = [0, 1]$) and (b) in the good confinement region ($\rho_{\rm norm} \in [\rho^{\rm min}_{\rm norm}, \rho^{\rm max}_{\rm norm}] = [0.3, 0.8]$). Discharges that belong to the L and H mode phases from the ITER Profile Database are shown.

is not included in our model. Regarding H mode discharges, the simulations have been performed imposing the boundary conditions for the temperatures at $\rho_{\rm norm} = 0.8$, i.e. at a value of the normalized radius that is generally inside the 'pedestal' region. A general trend of underestimating the simulated stored energies in H mode discharges is also observed from Fig. 7. This suggests that an optimal calibration of the free coefficients of our model (Eqs (9a, b)) could be performed in order to obtain more satisfactory results for the two distinct confinement modes considered.

3.2. JET hot ion and PEP discharges

In this section, we analyse JET discharges that belong to enhanced confinement regimes in which there is evidence that the thermal diffusion is reduced in the central region. We will also compare the results of the proposed model with the results of the mixed Bohm–gyro-Bohm model proposed by Erba et al. [12], in which no dependence on shear is included.

A list of the principal parameters characterizing the discharges is presented in Table II. The analysis of the discharges will be performed only for the L mode phase, before the transition to the H mode phase. All these discharges show an improvement of the confinement in the central region of the plasma, where a very low or even reversed magnetic shear is present. The improvement of the confinement is reflected in a strong thermal barrier appearing in the temperature profiles between one third and one half the radius of the plasma column (in particular, on the ion temperature profiles).

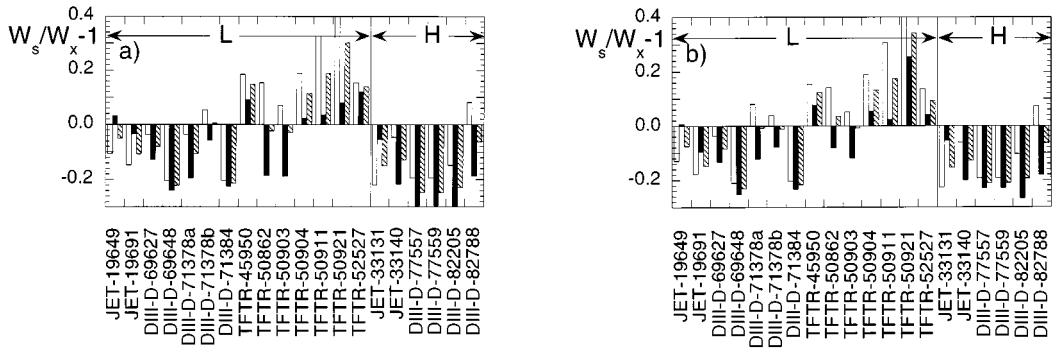

FIG. 7. $W_s/W_x - 1$ for electrons (white columns), ions (black columns) and electrons plus ions (hatched columns) (W_s and W_x are, respectively, the simulated and experimental stored thermal energies): (a) on the whole cross-section ($\rho_{norm} \in [\rho_{norm}^{min}, \rho_{norm}^{max}] = [0, 1]$) and (b) in the good confinement region ($\rho_{norm} \in [\rho_{norm}^{min}, \rho_{norm}^{max}] = [0.3, 0.8]$). Discharges that belong to the L and H mode phases from the ITER Profile Database are shown.

Table II. JET Hot Ion Discharges

Discharge	t (s)	$\langle n_e \rangle \times 10^{20}$ (m^{-3})	$T_e(0)$ (keV)	B_T (T)	I_p (MA)	$P_{NB,RF}$ (MW)
17749	44.6	0.37	9.4	3.2	3.07	5 (NB) + 11 (RF)
18757	52.9	0.11	9.0	3.2	3.10	10 (NB)
24464	45.5	0.36	4.7	3.3	3.01	12 (NB)
38480	46.8	0.16	13.1	3.6	2.90	10 (NB) + 10 (RF)

The thermal coefficients for electrons and ions proposed by Erba et al. [12], and which refer to a mixed Bohm–gyro-Bohm model without a magnetic shear dependence, are shown hereafter,

$$\chi_e^{mixed} = \alpha_{B,e}^{mixed} D_B \frac{1}{L_{p_e}^*} q^2 + \alpha_{gB}^{mixed} D_B \rho^* \frac{1}{L_{T_e}^*} \quad (11a)$$

$$\chi_i^{mixed} = \alpha_{B,i}^{mixed} D_B \frac{1}{L_{p_e}^*} q^2 + \alpha_{gB}^{mixed} D_B \rho^* \frac{1}{L_{T_e}^*} + \chi_{neo} \quad (11b)$$

where χ_{neo} is the neoclassical ion thermal diffusion coefficient [29] and the three calibration constants have been tuned for a typical L mode JET discharge,

$$\alpha_{B,e}^{mixed} = 4.0 \times 10^{-3}, \qquad \alpha_{B,i}^{mixed} = 2\alpha_{B,e}^{mixed} \quad (12a,b)$$

$$\alpha_{gB}^{mixed} = 7.84 \times 10^{-1}. \quad (12c)$$

Here $L_p^* \equiv |\nabla p|/p$ is the characteristic length of the pressure profile p normalized to the minor radius of the plasma column.

In Fig. 8, the standard deviations $\sigma_{T_e}, \sigma_{T_i}$ are shown, as obtained by simulating the JET discharges listed in Table II using the mixed, shear dependent model proposed in this article and the mixed model proposed by Erba et al. [12]. The mean values of the temperature standard deviation for all the discharges simulated are the following:

$$\langle \sigma_{T_e}^{mixed\ shear} \rangle \Big|_0^1 = 0.16, \quad \langle \sigma_{T_i}^{mixed\ shear} \rangle \Big|_0^1 = 0.16$$

$$\langle \sigma_{T_e}^{mixed} \rangle \Big|_0^1 = 0.26, \quad \langle \sigma_{T_i}^{mixed} \rangle \Big|_0^1 = 0.29.$$

The model proposed in this article gives results below $\approx$25%, whereas the mixed model without shear dependence gives results up to $\approx$40%. In addition, the electron, ion and total (electrons plus ions) stored thermal energies are shown in Fig. 9 for the same set of discharges. The mean values of W_s/W_x for all the discharges simulated and the quantities ΔR_W are the following:

$$\left\langle \frac{W_{s,e}^{mixed\ shear}}{W_{x,e}} \right\rangle \Big|_0^1 = 0.99$$

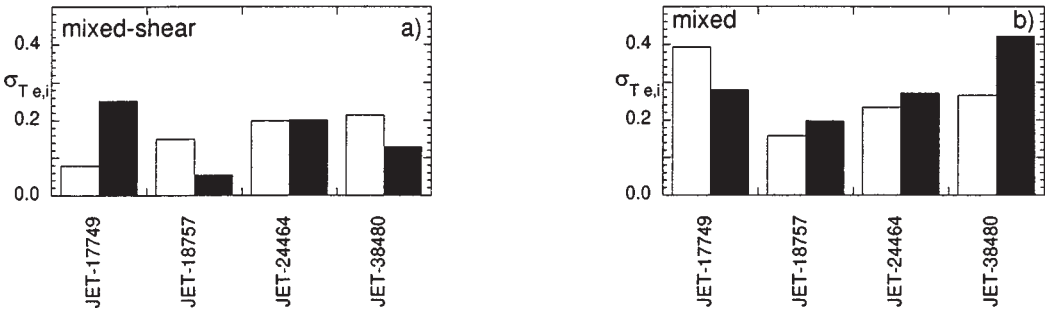

FIG. 8. Electron (white columns) and ion (black columns) temperature standard deviations for the JET hot ion and PEP discharges calculated on the whole cross-section ($\rho_{\rm norm} \in [\rho^{\rm min}_{\rm norm}, \rho^{\rm max}_{\rm norm}] = [0, 1]$). The mixed, shear dependent model (a) proposed in this article is compared with the mixed model (b) proposed in Ref. [12].

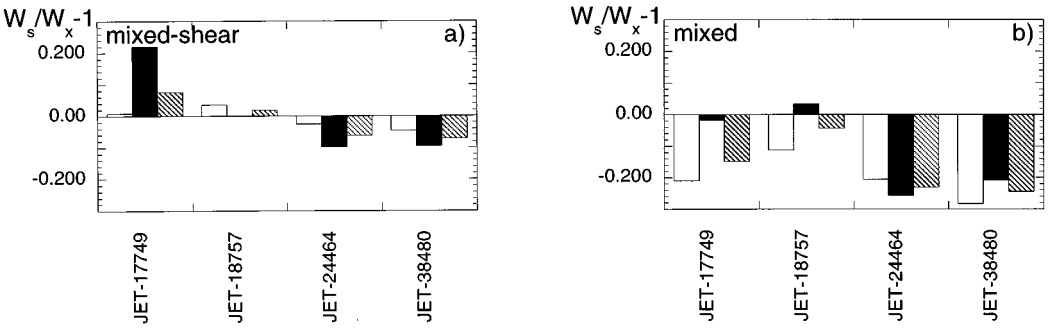

FIG. 9. $W_{\rm s}/W_{\rm x} - 1$ for electrons (white columns), ions (black columns) and electrons plus ions (hatched columns) ($W_{\rm s}$ and $W_{\rm x}$ are, respectively, the simulated and experimental stored thermal energies) for the JET hot ion and PEP discharges calculated on the whole cross-section ($\rho_{\rm norm} \in [\rho^{\rm min}_{\rm norm}, \rho^{\rm max}_{\rm norm}] = [0, 1]$). The mixed, shear dependent model (a) proposed in this article is compared with the mixed model (b) proposed in Ref. [12].

$$\left\langle \frac{W_{\rm s,i}^{\rm mixed\ shear}}{W_{\rm x,i}} \right\rangle \Bigg|_0^1 = 1.01$$

$$\left\langle \frac{W_{\rm s}^{\rm mixed\ shear}}{W_{\rm x}} \right\rangle \Bigg|_0^1 = 0.99$$

$$\Delta R_{W,{\rm e}}^{\rm mixed\ shear} \Big|_0^1 = 3.23\%$$

$$\Delta R_{W,{\rm i}}^{\rm mixed\ shear} \Big|_0^1 = 12.96\%,\ \Delta R_{W}^{\rm mixed\ shear} \Big|_0^1 = 6.15\%$$

$$\left\langle \frac{W_{\rm s,e}^{\rm mixed}}{W_{\rm x,e}} \right\rangle \Bigg|_0^1 = 0.80,\quad \left\langle \frac{W_{\rm s,i}^{\rm mixed}}{W_{\rm x,i}} \right\rangle \Bigg|_0^1 = 0.89$$

$$\left\langle \frac{W_{\rm s}^{\rm mixed}}{W_{\rm x}} \right\rangle \Bigg|_0^1 = 0.83,\quad \Delta R_{W,{\rm e}}^{\rm mixed} \Big|_0^1 = 21.15\%$$

$$\Delta R_{W,{\rm i}}^{\rm mixed} \Big|_0^1 = 16.67\%,\quad \Delta R_{W}^{\rm mixed} \Big|_0^1 = 18.47\%.$$

The improvement obtained by considering the dependence on the magnetic shear in the transport coefficients is evident (it has to be noted that the model proposed by Erba et al. [12] applied to the standard JET and DIII-D L mode discharges considered in Section 3.1 gives results that are similar to the mixed, shear dependent model proposed here). In particular, the ion temperature profile is always well reproduced by the mixed, shear dependent model, the model being able to closely follow the thermal barrier shown between one third and one half the radius of the plasma column. The experimental electron temperature profile shows a thermal barrier only on the discharge 17749 (this discharge also has a q profile with a negative shear for $\rho < 0.4$), and in this case the result of the mixed, shear dependent model is excellent. The ion temperature is in this case slightly overestimated, even though the profile is well reproduced. In Fig. 10, a comparison between the

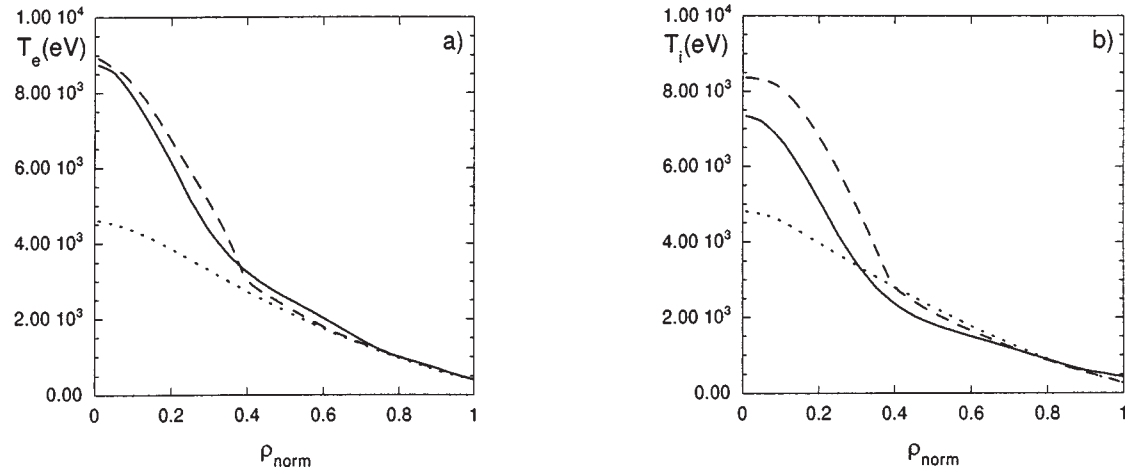

FIG. 10. Experimental (solid curves) and computed (dashed curves, mixed, shear dependent model proposed in this article; dotted curves, mixed model proposed in Ref. [12]) electron (a) and ion (b) temperature profiles for JET discharge 17749 at $t \simeq 44.6$ s.

experimental temperature profiles and those predicted by the mixed, shear dependent model and the mixed model proposed by Erba et al. [12] is presented. The radial profiles of the safety factor, magnetic shear and function $f(s)$ (Fig. 11) as obtained using the mixed, shear dependent model and the thermal diffusion coefficients (Fig. 12) are shown. Note the negative shear in the central part of the discharge (Fig. 11).

In the other discharges (which, incidentally, have very low shear in the central region, but monotonic q profiles), the thermal barrier on the electron temperature profiles is not as pronounced or is even not present at all, whereas it tends to appear in the simulated profiles obtained using the mixed, shear dependent model (e.g., Figs 13 and 14), which nevertheless show a very good agreement in comparison with the experimental profiles. This suggests that better agreement with the experimental results could be obtained by treating the shear dependence of the electrons differently from that of the ions in the thermal diffusion coefficient expressions.

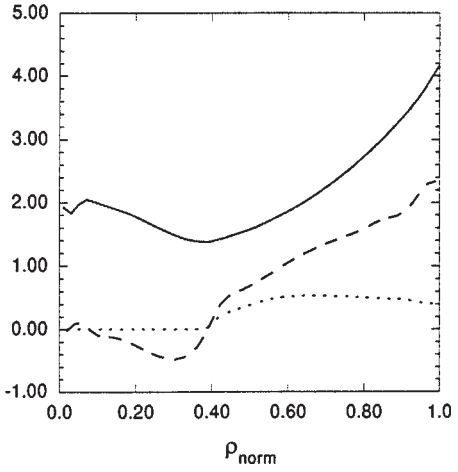

FIG. 11. Safety factor q (solid curve), shear (dashed curve) and shear dependent function $f(s)$ (dotted curve) radial profiles for the same discharge as Fig. 10.

4. CONCLUSIONS

In this article, a mixed Bohm–gyro-Bohm, shear dependent thermal diffusion coefficient has been proposed for L and H mode tokamak discharges. It has been heuristically derived on the basis of recent findings on the radial correlation length of turbulent processes generated by small scale, collisionless, electrostatic microinstabilities [14]. In particular, the thermal diffusion coefficient proposed here models a transport dominated by a Bohm contribution in the radial region of the plasma column where the magnetic shear is finite and by a gyro-Bohm contribution where the magnetic shear is small or even becomes negative.

Several standard L and H mode discharges from the ITER Profile Database [31] have been analysed

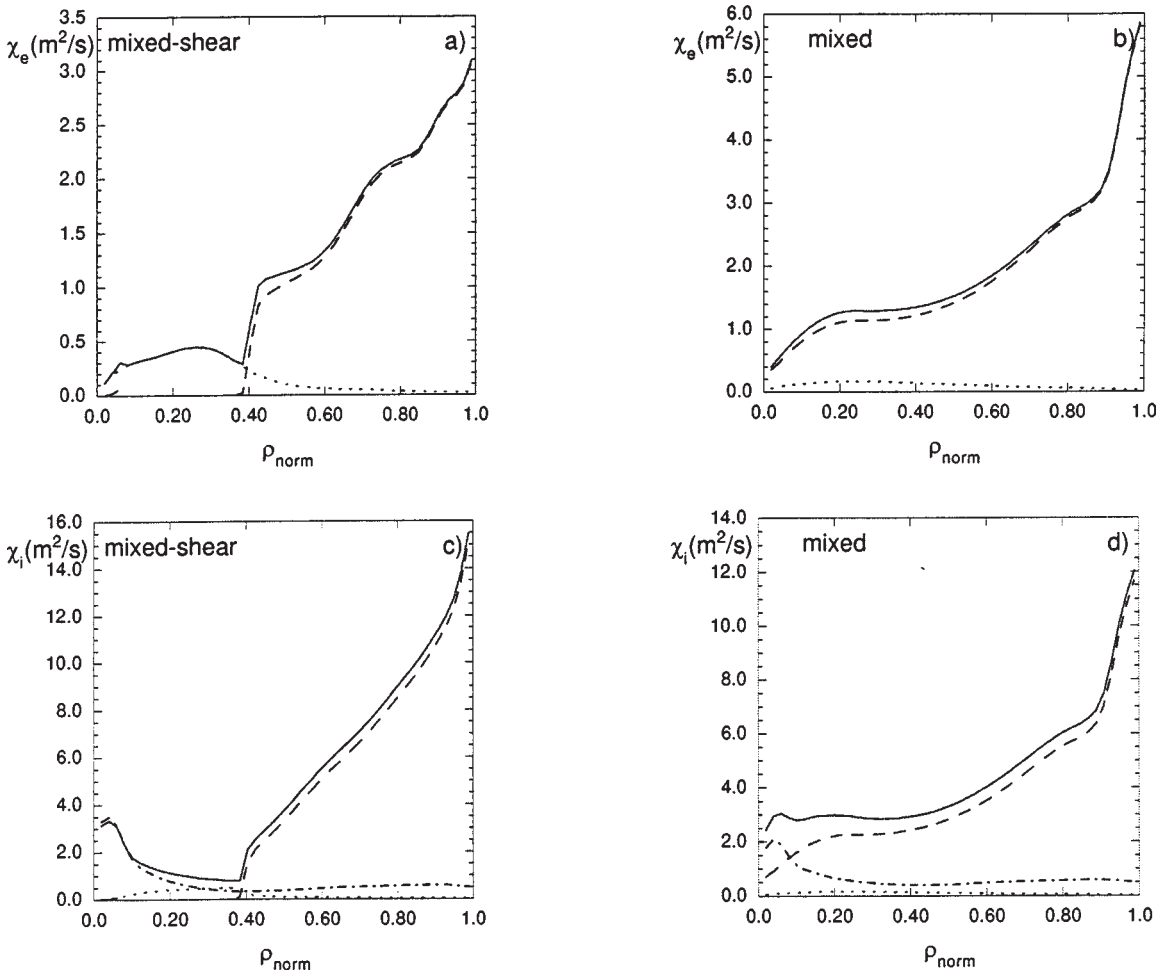

FIG. 12. Total (solid curves), Bohm (dashed curves), gyro-Bohm (dotted curves) and ion neoclassical (chain curves) thermal diffusivity radial profiles for (a, b) electrons and (c, d) ions for the same discharge as Fig. 10. The label 'mixed shear' refers to the diffusivity model proposed in this article, whereas the label 'mixed' refers to the model proposed in Ref. [12].

and the proposed transport model has produced very good results (with the exception of the DIII-D discharge 71378a, which is characterized by an off-axis neutral beam deposition profile). The mixed Bohm–gyro-Bohm, shear dependent thermal diffusion coefficients proposed have also been used to simulate the so-called hot ion mode discharges and PEP discharges obtained on JET. These discharges show an improvement of the confinement in the central region of the plasma, where a very low or even reversed magnetic shear is present. The results of our model are very promising, in particular for those types of discharge where a previously proposed mixed transport model without a magnetic shear dependence [12] does not give satisfactory results. It should be noted that the proposed transport model does not contain a self-consistent mechanism of 'pedestal' generation in the temperature profiles during H modes phases. In conclusion, the mixed Bohm–gyro-Bohm, shear dependent model seems to be very promising in simulating standard L and H mode discharges and interesting new confinement regimes like those characterized by very low or even negative magnetic shear.

ACKNOWLEDGEMENTS

The authors acknowledge the ITER JCT at San Diego and, in particular, Dr. D. Boucher as the person in charge of the ITER Profile Database and the groups that have made the experimental results available for this study.

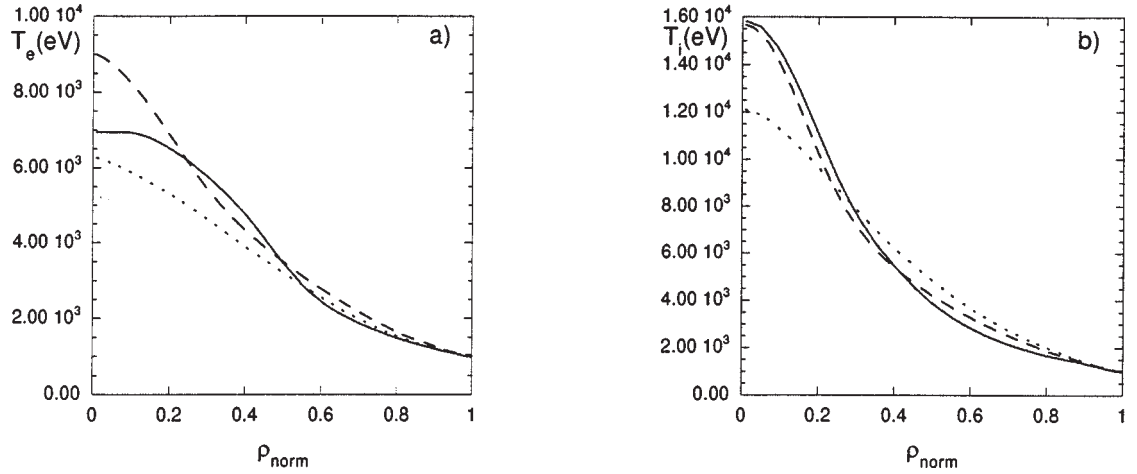

FIG. 13. Experimental (solid curves) and computed (dashed curves, mixed, shear dependent model proposed in this article; dotted curves, mixed model proposed in Ref. [12]) electron and ion temperature profiles for JET discharge 18757 at $t \simeq 52.9$ s.

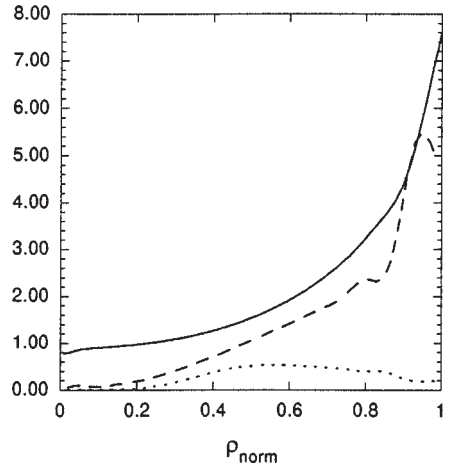

FIG. 14. Safety factor q (solid curve), shear (dashed curve) and shear dependent function $f(s)$ (dotted curve) radial profiles for the same discharge as Fig. 13.

REFERENCES

[1] KOTSCHENREUTER, M., DORLAND, W., BEER, M.A., HAMMETT, G.W., Phys. Plasmas **2** (1995) 2381.
[2] WALTZ, R.E., STAEBLER, G.M., HAMMETT, G.W., KONINGS, J.A., in Fusion Energy 1996 (Proc. 16th Int. Conf. Montreal, 1996), Vol. 2, IAEA, Vienna (1997) 385.
[3] OTTAVIANI, M., et al., Phys. Fluids B **2** (1990) 67.
[4] WEILAND, J., NORDMAN, H., Phys. Fluids B **5** (1993) 1669.
[5] SYDORA, R.D., DECYK, V.K., DAWSON, J.M., Plasma Phys. Control. Fusion **38** (1996) A281.
[6] ROMANELLI, F., TANG, W.M., WHITE, R.B., Nucl. Fusion **26** (1986) 1515.
[7] PETTY, C.C., et al., Phys. Plasmas **2** (1995) 2342.
[8] CHRISTIANSEN, J.P., et al., Nucl. Fusion **33** (1993) 863.
[9] BALET, B., et al., in Controlled Fusion and Plasma Physics (Proc. 22nd Eur. Conf. Bournemouth, 1995), Vol. 19C, Part I, European Physical Society, Geneva (1995) 9.
[10] HAWRYLUK, R.J., et al., Plasma Phys. Control. Fusion **33** (1991) 1509.
[11] KINSEY, J., BATEMAN, G., Phys. Plasmas **3** (1996) 3344.
[12] ERBA, M., CHERUBINI, A., PARAIL, V.V., SPRINGMANN, E., TARONI, A., Plasma Phys. Control. Fusion **39** (1997) 261.
[13] TARONI, A., ERBA, M., SPRINGMANN, E., TIBONE, F., Plasma Phys. Control. Fusion **36** (1994) 1629.
[14] ROMANELLI, F., ZONCA, F., Phys. Fluids B **5** (1993) 4081.
[15] CONNOR, J.W., TAYLOR, J.B., WILSON, H.R., Phys. Rev. Lett. **70** (1993) 1803.
[16] LAURO-TARONI, L., CONNOR, J.W., GIANNELLA, R., ROMANELLI, F., WILSON, H.R., in Controlled Fusion and Plasma Physics (Proc. 22nd Eur. Conf. Bournemouth, 1995), Vol. 19C, Part I, European Physical Society, Geneva (1995) 89.
[17] BALET, B., et al., Nucl. Fusion **30** (1990) 2029.
[18] GREENWALD, M., et al., Phys. Rev. Lett. **53** (1984) 352.

[19] ALLADIO, F., et al., Plasma Phys. Control. Fusion **35** (1993) B241.
[20] GÉRAUD, A., et al., in Controlled Fusion and Plasma Physics (Proc. 21st Eur. Conf. Montpellier, 1994), Vol. 18B, Part I, European Physical Society, Geneva (1994) 298.
[21] HOANG, G.T., et al., ibid., Part III, p. 1054.
[22] STRAIT, E.J., et al., Phys. Rev. Lett. **75** (1995) 4421.
[23] ZARNSTORFF, M.C., et al., in Plasma Physics and Controlled Nuclear Fusion Research 1990 (Proc. 13th Int. Conf. Washington, DC, 1990), Vol. 1, IAEA, Vienna (1991) 109.
[24] CHALLIS, C.D., et al., Nucl. Fusion **32** (1992) 2217.
[25] PERKINS, F.W., et al., Phys. Fluids B **5** (1993) 477.
[26] BRETZ, N.L., et al., in Plasma Physics and Controlled Nuclear Fusion Research 1992 (Proc. 14th Int. Conf. Würzburg, 1992), Vol. 1, IAEA, Vienna (1992) 551.
[27] TANG, W.M., REWOLDT, G., Phys. Fluids B **5** (1993) 2451.
[28] CONNOR, J.W., Plasma Phys. Control. Fusion **37** (1995) A119.
[29] CHANG, C.S., HINTON, F.L., Phys. Fluids **29** (1986) 3314.
[30] CENACCHI, G., TARONI, A., in Computational Physics. Computing in Plasma Physics (Proc. 8th Europhysics Conf. Eibsee, 1986), Vol. 10D, European Physical Society, Geneva (1986) 57.
[31] CONNOR, J.W., et al., in Fusion Energy 1996 (Proc. 16th Int. Conf. Montreal, 1996), Vol. 2, IAEA, Vienna (1997) 935.

(Manuscript received 8 May 1997
Final manuscript accepted 9 December 1997)

E-mail address of G. Vlad:
vlad@frascati.enea.it

Subject classification: F2, Tt; F2, Ti